Acta Mechanica Sinica (2019) 35(4):839–851
https://doi.org/10.1007/s10409-019-00859-w

RESEARCH PAPER

Dynamic crushing of cellular materials: a particle velocity-based analytical method and its application

Shilong Wang[1] · Zhijun Zheng[2] · Yuanyuan Ding[3] · Changfeng Zhu[2] · Jilin Yu[2]

Received: 29 September 2018 / Revised: 25 December 2018 / Accepted: 20 February 2019 / Published online: 30 April 2019
© The Chinese Society of Theoretical and Applied Mechanics and Springer-Verlag GmbH Germany, part of Springer Nature 2019

Abstract
Cellular material under high-velocity impact exhibits a typical feature of layerwise collapse. A cell-based finite element model is employed herein to simulate the direct impact of a closed-cell foam, and one-dimensional velocity field distributions are obtained to characterize the crushing band propagating through a cellular material. An explicit expression for the continuous velocity distribution is derived based on the features of the velocity gradient distribution. The velocity distribution function is adopted to determine the dynamic stress–strain states of cellular materials under dynamic loading. The local stress–strain history distribution reveals that sectional cells experience a process from the precursor elastic behavior to the shock stress state, passing through the dynamic initial crushing state. A power-law relation between the dynamic initial crushing stress and the strain rate is established, which confirms the strain rate effect of cellular materials. By extracting the critical points immediately before the unloading stage in the local dynamic stress–strain history curves, the dynamic stress–strain states of cellular materials are determined. They exhibit loading rate dependence but are independent of the initial impact velocity. Furthermore, with increase of the relative density, the dynamic hardening behavior of the cellular specimen is enhanced and the crushing process event is advanced. The particle velocity-based analytical method is applied to analyze the dynamic responses of cellular materials. This method is better than continuum-based shock models, since it does not require a preassumed constitutive relation. Therefore, the particle velocity-based analytical method proposed herein may provide new ideas to carry out dynamic experimental measurements, which is especially applicable to inhomogeneous materials.

Keywords Cellular material · Velocity distribution · Dynamic behavior · Strain rate effect · Dynamic stress–strain state

1 Introduction

Cellular materials, such as aluminum foams and honeycombs, have high porosity and exhibit excellent performance in terms of their energy absorption capability. In practical applications of impact energy absorbers and antiblast structures, adverse energies applied externally are attenuated by cellular materials with nearly unchanged support stress [1–4] to ensure that the contained payload is protected. Highly localized deformation is one typical feature of cellular materials under dynamic impact. Usually, a structural stress wave is adopted to characterize the propagation of the localized crushing band in such materials [5]. Correspondingly, a series of shock models have been proposed to analyze the dynamic responses of cellular materials [6–11]. However, since cellular materials are inhomogeneous and have intrinsic characteristic scales, the applicability of continuum-based shock models to analyze the dynamic response of this kind of material inevitably results in differences from the real behavior of wave propagation through cellular materials [8]. Moreover, these models describe the quasistatic mechanical behavior on the homogeneous scale, while the application of a shock wave within a homogenized medium to effectively characterize the dynamic crushing behavior of cellular materials requires further discussion.

Considering the difficulty in measuring the local stress and strain states of cellular materials under dynamic impact experimentally, Liao et al. [12] developed a local strain calculation

✉ Zhijun Zheng
zjzheng@ustc.edu.cn

[1] School of Civil Engineering, Anhui University of Technology, Ma'anshan 243032, China

[2] CAS Key Laboratory of Mechanical Behavior and Design of Materials, Department of Modern Mechanics, University of Science and Technology of China, Hefei 230026, China

[3] Mechanics and Materials Science Research Center, Ningbo University, Ningbo 315211, China

method based on the optimal local deformation gradient. As a practical example, the strain field distributions of irregular honeycombs under in-plane loading were calculated, which can well capture the propagation of the stress wave [13]. To study the dynamic behavior of cellular materials experimentally, the dynamic evolution of the deformation in open-cell aluminum foams was monitored and the local physical quantities were measured with the aid of high-speed photography coupled with digital image correlation (DIC) [14]. Hugoniot relations between the dynamic response (i.e., shock wave speed, stress, and strain) and impact velocities were then established. It is worth noting that a linear Hugoniot relation between the shock wave speed and corresponding impact velocity was obtained, as also reported in Refs. [15–17]. In combination with the conservation of mass and momentum across the shock front, the dynamic stress–strain states can then be determined conveniently. However, such an analytic model is based on the assumption that the stress ahead of the shock front has the same level as the first local stress maximum of the quasistatic stress–strain curve. However, the stress immediately ahead of the shock front, i.e., the dynamic initial crushing stress, is actually not a constant value but has a distribution away from the distal end [18]. Besides, the dynamic initial crushing stress also exhibits strain rate sensitivity, which is essentially different from the quasistatic state [15, 19]. Therefore, the dynamic stress–strain states of cellular materials were obtained numerically using a different approach based on the strain field distribution by Zheng et al. [11]. The obvious distinction between the dynamic and quasistatic stress–strain relations was attributed to the different deformation mechanisms. Layerwise crushing bands form in cellular materials depending on the speed of the shock wave during dynamic crushing, while shear bands occur randomly under quasistatic loading, which indicates that the dynamic behavior of cellular materials is velocity dependent. Substantially, the dynamic constitutive behavior of cellular materials is deformation mode dependent.

Recently, the stream of literature on the evolution of the dynamic behavior of cellular materials was systematically reviewed to highlight the commonality and contrasts in terms of the phenomena and mechanisms, and their modeling [20]. This historical perspective shows that much knowledge has been acquired on the dynamic crushing behavior of cellular materials. However, there is no effective and convenient way to determine the dynamic stress–strain state of cellular materials yet, especially for experimental tests, since experimental data are difficult to measure due to issues associated with the highly localized deformation and the limitations of experimental techniques. The dynamic rigid-plastic hardening (D-R-PH) idealization [11] can be expressed as

$$\sigma(\varepsilon) = \sigma_0^{\mathrm{d}} + \frac{D\varepsilon}{(1-\varepsilon)^2}, \tag{1}$$

where D is the dynamic strain hardening parameter and σ_0^{d} is the dynamic initial crush stress. Consequently, the two-parameter dynamic material model exhibits powerful ability to characterize the dynamic stress–strain states and may lead to ideas to determine the dynamic mechanical behavior of cellular materials using a feasible method. Following this route, the effects of the relative density, entrapped gas, and hardening behavior of the base material on the shock properties of cellular materials were investigated practically by carrying out virtual tests [21], providing further understanding of the mechanisms underlying such effects of mesostructural features. Since the shock model is established on the condition of shock initiation, the intermediate state of cellular materials cannot be well elucidated by such theoretical idealization.

The treatment of the macroscopic discontinuity at the crushing front constitutes the basis of the description of the dynamic behavior of cellular materials using shock theory [22]. However, the shock front where crushed cells start to form always has a finite thickness [18, 23] in reality. To portray the dynamic behavior of cellular materials more realistically, the Lagrangian analysis method can be adopted to investigate the local dynamic response of three-dimensional (3D) Voronoi structures under a Taylor impact [19]. By considering the critical points on local dynamic stress–strain curves, a unique dynamic stress–strain state curve that is related to different loading rates can be extracted without any preassumed constitutive relations. When this Lagrangian analysis method is directly applied to experimental tests on foams, a tremendous amount of data on the historical particle velocity distribution is required to ensure the accuracy of results, since differential equations must essentially be solved, which is hard to realize due to the limitations of experimental techniques. Therefore, a convenient method that could be used to draw ideas effectively from dynamic tests on cellular materials is pressingly desired.

In this paper, the dynamic behavior of cellular materials is further studied using the particle velocity distribution to reveal the mesodeformation mechanism. The aim is to propose an analytical model for the velocity distribution for application in calculations of the history distribution of the dynamic local stress and local strain. Finally, the dependence of the dynamic behavior of cellular materials on the relative density is investigated using the proposed analytical model.

2 Numerical simulations

2.1 Cell-based finite element model

A closed-cell foam model (Fig. 1a) is generated using the 3D Voronoi technique [24]. Firstly, a set of distinct and isolated

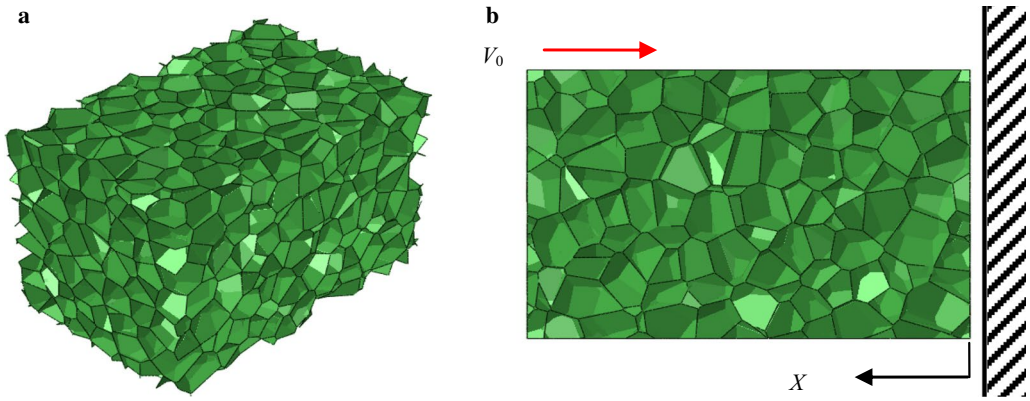

Fig. 1 **a** Finite element model of closed-cell foam, **b** direct impact scenario

points are randomly generated in a 3D region based on the principle that the distance between any two points is not less than a given distance. Secondly, a Delaunay tessellation [25] is constructed by generating a triangulation that maximizes the minimum angle of all the angles of the triangles. Thirdly, Voronoi polyhedra are obtained by generating the intersections of the planes orthogonal to the edges of all the Delaunay tetrahedra passing through the midpoints of these edges. Finally, a Voronoi diagram is obtained and trimmed to obtain a Voronoi structure. The Voronoi configuration can characterize the mesostructure of some kinds of cellular foam well and thus is widely employed in numerical simulations to understand the mechanical behavior of cellular materials [17, 26–29].

The cellular specimen model used in this study contains 600 nuclei in a volume of 20 mm × 20 mm × 30 mm with cell irregularity of 0.4. The average cell size d_c, defined as the diameter of a sphere whose volume is equal to the average volume of the cells within the Voronoi structure, is about 3.2 mm. The cell-wall material of the cellular specimen is assumed to be elastic–perfectly plastic with density $\rho_s = 2700$ kg/m^3, Young's modulus $E = 69$ GPa, Poisson's ratio $\nu = 0.3$, and yield stress $\sigma_{ys} = 170$ MPa. The cell-wall thickness of the cellular specimen is uniform and is dependent on the relative density of the specimen ρ, which is defined as the ratio of the cellular specimen density ρ_f to the cell-wall material density ρ_s. In this study, the relative density of the cellular specimen is set as 0.1, which gives a cell-wall thickness as 0.095 mm. The ABAQUS/Explicit finite element code [30] is used to perform the numerical simulations. The cell walls of the Voronoi structure are meshed with shell elements of type S3R and S4R. After mesh convergence analysis, the element size is taken as 0.3 mm [21]. Thus, the cellular specimen used in study has about 30,872 S3R elements and 109,119 S4R elements.

A direct impact scenario is applied in the numerical simulations. During numerical testing, the specimen impinges onto a fixed rigid plate with initial impact velocity V_0, as shown in Fig. 1b. A linear multipoint constraint is applied to the surfaces in the impact direction to avoid rollover of the specimen under high-velocity impact. The general contact is applied to satisfy the complex contact behaviors among any possible contact surfaces with a friction coefficient of 0.2.

2.2 Calculation method for velocity field distribution

The cellular specimen under dynamic impact exhibits highly localized deformation; i.e., the collapse of cells initiates within a narrow band while the cells ahead of the collapse band remain almost undeformed. As the loading event continues, the collapse band spreads from the impact end to the free end layer by layer, as shown in Fig. 2. The propagation of the collapse band happens in nearly flat planes with negligible lateral expansion. Herein, the investigation of the impact behavior of the cellular specimen can be simplified to the issue of one-dimensional wave propagation. As a basic physical quantity, the velocity field can be applied to characterize the status of the cellular structure. Besides, the velocity components along the impact direction can be extracted directly from the numerical results, enabling convenient and reliable calculation of the local velocity field. A middle section parallel to the impact direction is selected to investigate the deformation evolution during impact. A sequence of local velocity field distributions in the framework of the Lagrangian coordinate is determined, and the corresponding mesodeformation patterns of the cut section of the cellular specimen with initial impact velocity $V_0 = 250$ m/s extracted, as shown in Fig. 2. It transpires that the shock-like deformation is captured well by the velocity field distribution. During crushing, the kinetic energy of the cellular specimen is progressively dissipated in the form of plastic collapse of cell walls, which results in a gradual reduction of the impact velocity of the undeformed portion.

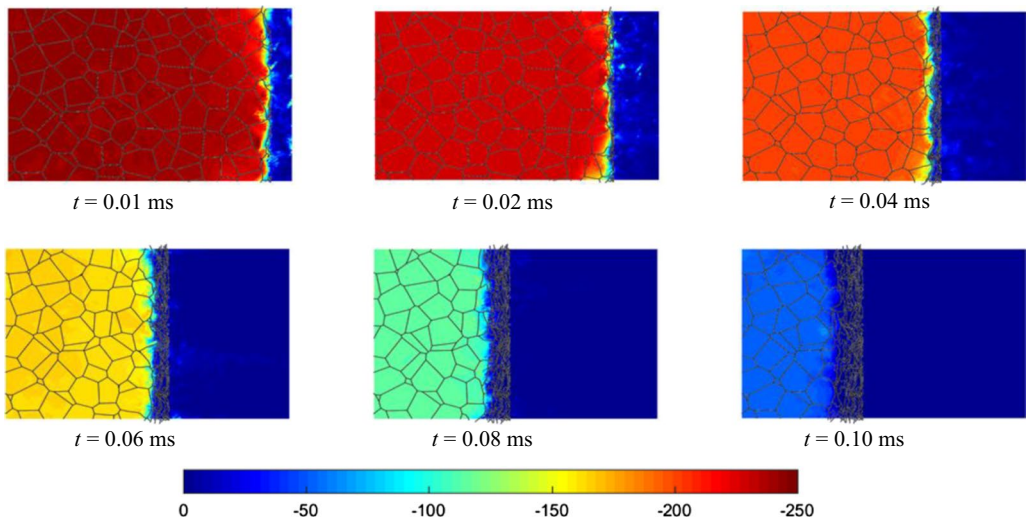

Fig. 2 Velocity distribution fields in impact direction of cellular specimen together with corresponding deformation configurations

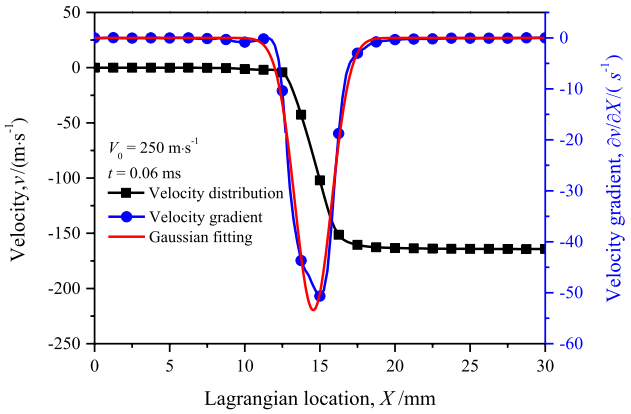

Fig. 3 1D velocity distribution and corresponding velocity gradient

The one-dimensional (1D) velocity distribution can be determined by averaging the velocity components along the longitudinal direction of the specimen at each Lagrangian position within a range of one cell size at a specific moment, as shown in Fig. 3. A three-point centered difference is adopted to determine the local velocity gradient distribution. It is demonstrated that the macroscopic deformation status of the cellular specimen under impact can be basically separated into three regions: the crushed section, the crushing initiation section, and the undeformed section. The crushing initiation section spans a range of about one cell diameter, where the cells transform dramatically from an undeformed to compacted state, as depicted in Fig. 3. Macroscopically, the propagation of the crushing front behaves as a shock wave, so it is usually treated as a singular plane to propose shock models in the framework of continuum mechanics. To date, a series of shock models have been proposed to characterize the crushing behavior of cellular materials [10, 11, 31].

3 Particle velocity-based analysis

The 1D velocity gradient distribution at a specific moment exhibits a bell-shaped feature, as illustrated in Fig. 3. According to this feature, the Gaussian unimodal distribution is applied to characterize the velocity gradient distribution, expressed as

$$\frac{\partial v}{\partial X} = \alpha \mathrm{e}^{-\left(\frac{X-b}{w}\right)^2}, \tag{2}$$

where α, b, and w are substantially understood as the change of the instantaneous impact velocity, the Lagrangian location of the extreme value on the velocity gradient distribution, and the width of the crushing initiation section, respectively. It is worth noting that this Gaussian distribution description is not the only possible form of fitting function. However, the chosen function should offer a simple expression, easy solution, and physical clarity. Moreover, the sensitivity of the dynamic response to the fitting accuracy of the velocity gradient is presented in "Appendix A." Integrating Eq. (2) with respect to the Lagrangian location and considering the boundary condition $v=0$ at $X=0$ yields a spatial velocity distribution of

$$\begin{aligned} v(t,X) &= \alpha(t)\int_0^X \mathrm{e}^{-\left[\frac{\xi-b(t)}{w(t)}\right]^2}\mathrm{d}\xi \\ &= a(t)\left[\mathrm{erf}\left(\frac{X-b(t)}{w(t)}\right) - \mathrm{erf}\left(-\frac{b(t)}{w(t)}\right)\right], \end{aligned} \tag{3}$$

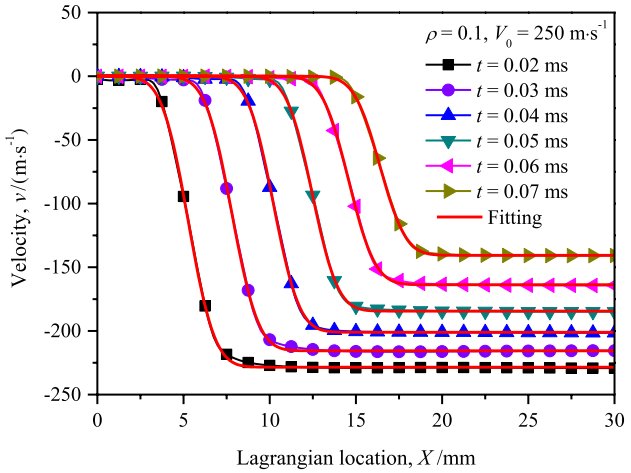

Fig. 4 1D velocity distribution obtained from numerical simulations and corresponding fitting

where erf(•) is the error function and $a(t) = -\sqrt{\pi}\alpha(t)w(t)/2$. The analytic model in Eq. (3) exhibits adaptable ability to capture the features of the velocity distribution of the cellular specimen at different impact moments extracted directly from the numerical results, as shown in Fig. 4.

Once the form of the velocity distribution function has been determined, the variations of the associated parameters with time can be investigated by applying Eq. (3) to the velocity distributions extracted from the numerical results, as shown in Fig. 5. The results indicate that both parameters a and b exhibit a nonlinear trend with impact time, while the parameter w increases linearly with the development of the crushing process. During impact, kinetic energy is gradually dissipated by collapse of cell walls, and the decreasing impact velocity attenuates the propagation of the crushing front while the width of the crushing initiation region expands. When the impact velocity is decreased to a critical velocity, the deformation exhibits a combination of layerwise crushing bands and random shear bands, which is known as the transition mode. In such case, the 1D simplification may overaverage the behaviors of the cellular specimen at moderate impact velocity. Herein, the method based on the spatial velocity distribution function to study the mechanical behavior of cellular materials is much more reliable for the loading case with sufficiently high impact velocity.

Considering the boundary condition $b(0) = 0$, low-order polynomial functions, i.e., $a(t) = a_1t^2 + a_2t + a_3$, $b(t) = b_1t^2 + b_2t$, and $w(t) = w_1t + w_2$, are adopted to fit the variations of the parameters with impact time, as demonstrated in Fig. 5, with fitting parameters of $a_1 = 7447$ mm·ms^{-3}, $a_2 = 201.8$ mm·ms^{-2}, $a_3 = -120.9$ mm·ms^{-1}, $b_1 = -848.1$ mm·ms^{-2}, $b_2 = 291.4$ mm·ms^{-1}, $w_1 = 0.7331$ mm·ms^{-1}, and $w_2 = 1.659$ mm. After determining the quantitative relations of the three parameters in Eq. (3), the general form of the spatial velocity distribution function can be rewritten as

$$v(t,X) = \left(a_1t^2 + a_2t + a_3\right) \times \left[\mathrm{erf}\left(\frac{X - b_1t^2 - b_2t}{w_1t + w_2}\right) - \mathrm{erf}\left(-\frac{b_1t^2 + b_2t}{w_1t + w_2}\right)\right], \tag{4}$$

where the seven undetermined coefficients correctly characterize the response of cellular materials with different properties (the relative density of the cellular material, and the properties of the base material and mesostructure). Note that Eq. (4) cannot satisfy the initial condition $v(0, X) = -V_0$. This incompatibility is attributed to the dispersion in the data due to the boundary effect as well as the neglect of the propagation and reflection of elastic wave in the early stage of the crushing event (see "Appendix B"). Therefore, the velocity-based model is highly applicable for investigating the dynamic behavior of cellular materials with a relatively stable crushing front. Together with the jump conditions (i.e., conservation of mass and momentum) across the shock front in Lagrangian form, the analytical velocity distribution can be applied to study the local dynamic evolution characteristics of the stress and strain, dynamic initial crushing stress, and dynamic stress–strain states of cellular materials during impact by extracting the velocity profiles at nodes from numerical or experimental results.

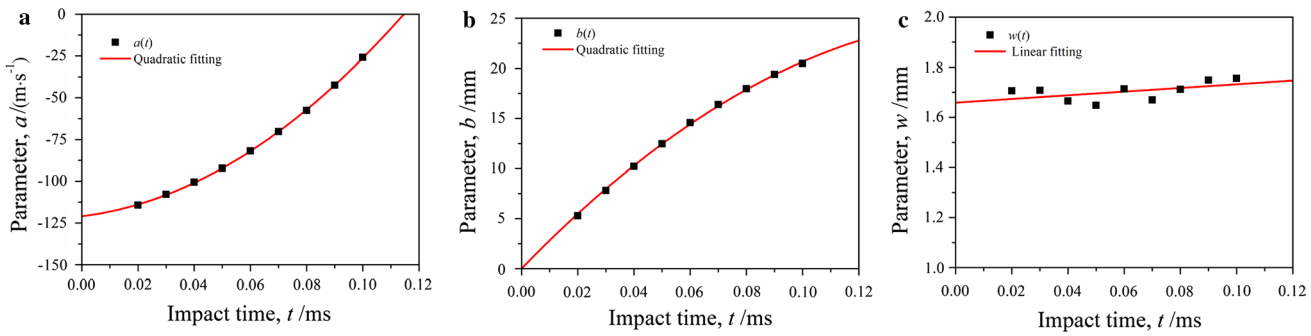

Fig. 5 Variations of parameters **a** a, **b** b, and **c** w in Eq. (3) with time

4 Results and discussion

4.1 Dynamic local stress and strain

In the theory of 1D stress wave propagation, the conservation equations for mass and momentum can be expressed in Lagrangian form as [32]

$$\frac{\partial v}{\partial X} = -\frac{\partial \varepsilon}{\partial t}, \tag{5}$$

and

$$\rho_f \frac{\partial v}{\partial t} = -\frac{\partial \sigma}{\partial X}, \tag{6}$$

where ε, σ, v and ρ_f are strain, stress, particle velocity, and initial density, respectively. Here, it is stipulated that the stress and strain are positive for the compressive case. Then, the dynamic behavior of the local strain in cellular materials can be obtained by combining Eqs. (4) and (5) with the initial condition $\varepsilon(0, X) = 0$. Similarly, the local stress can be determined from Eqs. (4) and (6) together with the boundary condition $\sigma(t, L_0) = 0$ (where L_0 is the initial length of the cellular specimen). Here, it is noteworthy that, for a cellular material examined using a cell-based model, the definition of local stress or local strain is the average response at a considered location over the range of an intrinsic characteristic length (i.e., the average cell size). In actual dynamic tests of cellular materials, velocity data recorded to analyze the response are not sufficient to guarantee the accuracy of such results due to the limitations of existing experimental techniques. Compared with the investigation of the dynamic behavior of cellular materials using the Lagrangian analysis method [19], the analytical method developed herein only requires particle velocity data at a few Lagrangian positions for different impact moments to determine the spatial velocity distribution function expressed in Eq. (4). The strain history and stress history can then be conveniently acquired using Eqs. (5) and (6). Accordingly, the solving method based on the spatial velocity distribution proposed herein provides a new approach to carry out experimental studies on the dynamic behavior of cellular materials.

The time history of local stress is calculated from Eqs. (4) and (6) with zero stress at the free end ($\sigma(0, t) = 0$), as shown in Fig. 6. These results indicate that each cross-section corresponding to a certain Lagrangian position will experience three stages successively: the elastic stage, the collapse stage, and the compacted stage. Once an impact event begins, collapse of cell walls happens immediately after the precursor elastic behavior, and the stress increases to the level of the initial crushing stress. Due to the attenuation of the impact strength and the interaction of the elastic unloading wave, the stress in the compacted region gradually decreases, exhibiting

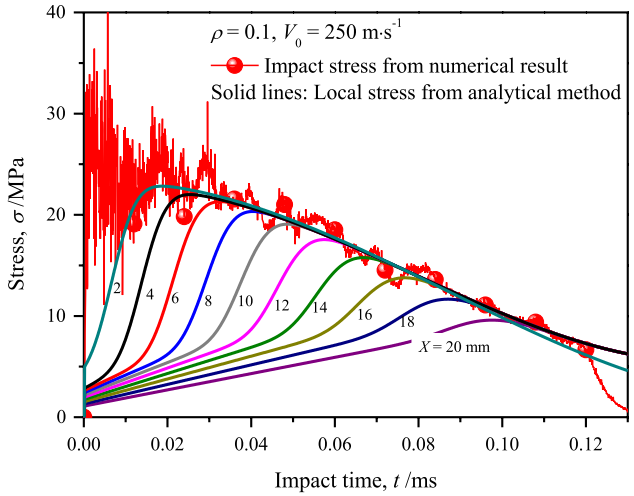

Fig. 6 Comparison of stress behind shock front obtained directly from finite element results with local stress calculated numerically

a negative correlation with distance from the impacted end, until the crushing event terminates completely. Note also that the upper envelope curve of the local stress histories coincides with the boundary stress history extracted directly from the numerical results. For the direct impact case, the compaction region through which the crushing front passes becomes part of the supported rigid plate. The inertia effect can be ignored, and the stress has a uniform distribution in this stationary region. Therefore, the reliability of the stress–time distribution determined by the analytical analysis method is further validated. However, there is nearly no oscillation phenomenon in the elastic stage compared with the trend of the distribution of the local stress history obtained by the Lagrangian analysis method [19]. Actually, the velocity distribution exhibits a transition from the instantaneous impact velocity in the compaction region to the final stationary state in the undeformed region, as shown in Fig. 4, which can probably be attributed to elastic bending waves [18]. The fitting used in the analytical method described herein eliminates the oscillation in the velocity distribution curve, resulting in linear behavior in this stage, as depicted in Fig. 6.

Similarly, using Eqs. (4) and (5), the time-history distribution of the strain at any Lagrangian position can be obtained by considering the initial condition $\varepsilon(X, 0) = 0$, as shown in Fig. 7. The locations with near-zero strain indicate cells that remain undeformed before arrival of the crushing front. The local strain field calculation method [12] is further adopted to verify the reliability of the local strain field distribution calculated by the analytical method proposed herein, as shown in Fig. 8. These results show that the strain fields determined by the two methods are in good agreement. This indicates the validity of this velocity-based analytical method for investigation of the dynamic response of cellular

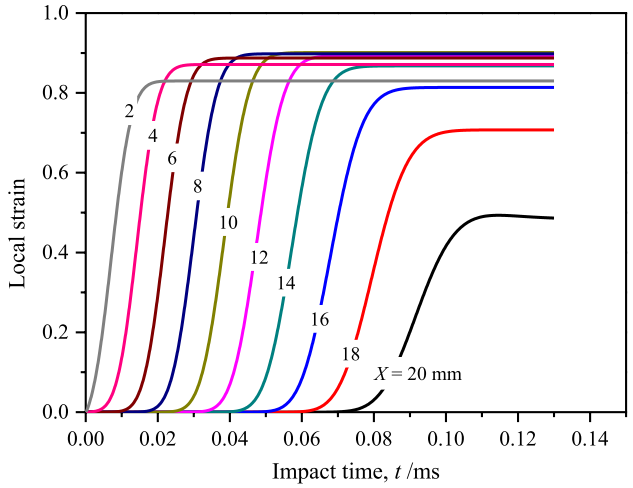

Fig. 7 Variation of local strain at Lagrangian locations with time

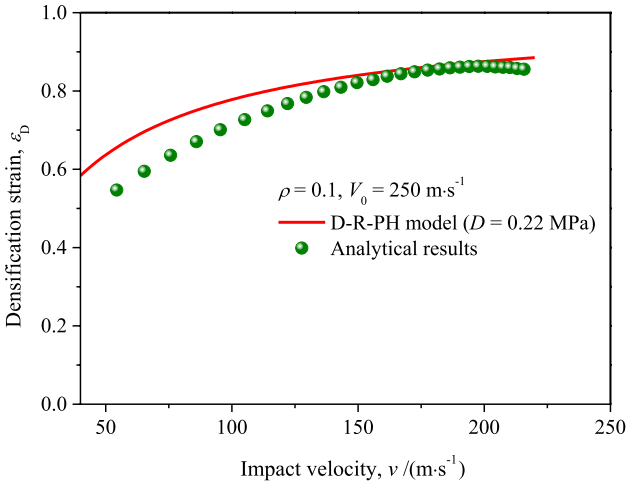

Fig. 9 Variation of densification strain with impact velocity

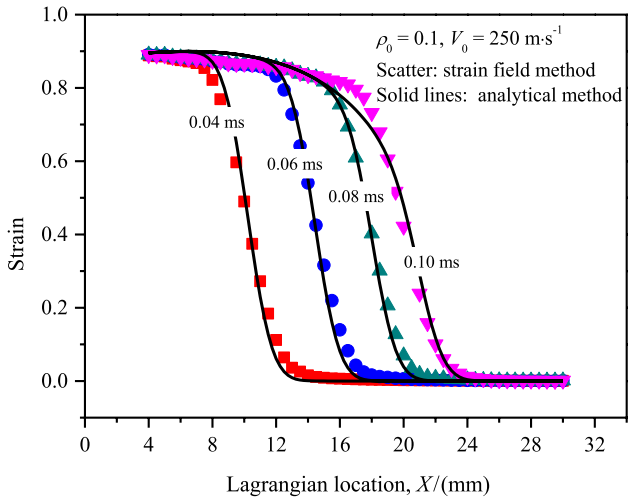

Fig. 8 Comparison of local strain field distributions obtained by the velocity-based analytical method and local strain field calculation method

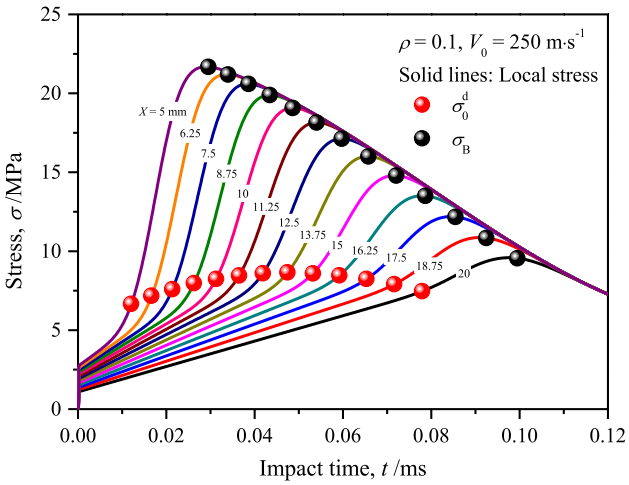

Fig. 10 Variation of local stress with impact time

materials. When the crushing front arrives at a specific section, the sectional strain increases dramatically to the level of the densification strain, which is related to the intensity of the instantaneous impact velocity, as shown in Fig. 9. This demonstrates that the densification strain behind the crushing front increases with increase of the impact velocity and finally asymptotically approaches a constant value that is dependent on the relative density of the cellular specimen. It is also interesting to note that, when the impact velocity is about 130 m/s, the densification strain increases slowly and basically coincides with the results determined from the D-R-PH shock model [11]. When the impact velocity is below 130 m/s, the densification strain is lower than the results predicted using the D-R-PH shock model, and the deviation becomes more significant as the impact velocity decreases to moderate values. Since the deformation mode of the cellular material is strongly dependent on the impact velocity, the validity of the shock model under moderate-velocity impact is questionable. A critical impact velocity to indicate the applicability of the D-R-PH model must be defined. For a Voronoi structure with relative density of 0.1, this critical impact velocity is taken as 130 m/s, although this is not a general result, since the velocity depends on the methods that are adopted to determine the dynamic behavior of cellular materials quantitatively, as described in "Appendix C."

The variation of the stress at certain Lagrangian positions is shown in Fig. 10. As the crushing front approaches, the location immediately ahead enters an initial crushing state and serves as a precursor for the incoming collapse behavior of the cells. Once the crushing front passes by, the compacted region behind the crushing front remains stationary

and the shock stress (the stress behind the crushing front) decreases with the drop of the impact velocity. One phenomenon to be noted is that a smooth trend in the local stresses occurs before the crushing front arrives compared with the oscillation in this stage obtained using the Lagrangian analysis method. As discussed above, the fitting treatment applied to the velocity distribution essentially neglects the effect of the elastic loading and unloading waves.

4.2 Strain rate effect of cellular material

The deformation mode of cellular materials exhibits strong impact velocity sensitivity, changing from random shear bands under quasistatic compression to layered crushing bands under high-velocity impact. Nevertheless, the impact velocity, which is not a material parameter, only serves as an extrinsic factor to relate with some intrinsic parameters of the materials (such as micro-inertia, cell morphology, or strain rate sensitivity of cell wall). The strain rate sensitivity of the peak stress and crushing stress of honeycombs was quantified numerically and analytically [33]. However, for cellular materials, there are conflicting conclusions regarding whether or not their dynamic behavior are sensitive to the strain rate. Dynamic tests were conducted on aluminum foams by Deshpande and Fleck [34] using a split Hopkinson pressure bar (SHPB) apparatus; the results indicated that the plateau stress of aluminum foams shows no strain rate sensitivity, even when the loading rate increases to $\dot{\varepsilon} = 5 \times 10^3\ \mathrm{s}^{-1}$. Conversely, Mukai et al. [35] reported that the enhancement of the plateau stress of closed-cell aluminum foams could reach about 50%–100% when the loading rate is over $\dot{\varepsilon} = 1 \times 10^3\ \mathrm{s}^{-1}$. When carrying out dynamic tests, the two coupled dynamic effects (i.e., strain rate effect and inertia effect) cannot be uncoupled well due to the highly localized deformation features under dynamic impact [36].

At a certain moment of the impact, the dynamic initial crushing stress is intuitively understood as the strength of the region of cellular material immediately ahead of the shock front during impact. However, the transition of the stress from the elastic to crushing region is gentle due to the delayed change of the material state. Instead, the Lagrangian location of the initial crushing stress σ_0^{d} can be determined by the intersection of the extrapolated linear lines of the undeformed part ahead of the crushing front and the crushing part where the cell collapse approximately happens. The corresponding strain rate at the current moment is then also determined from the local strain rate distribution, which is obtained by taking the derivative of the velocity distribution with respect to the Lagrangian coordinate, as shown in Figs. 11 and 12, respectively. Obviously, the definition of the local strain rate depends on the method used to determine the initial crushing stress. Since the initial crush state

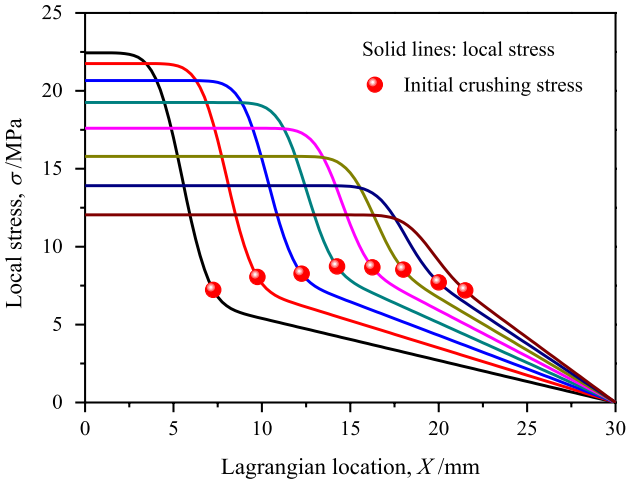

Fig. 11 Distribution of initial crushing stress with Lagrangian position at different moments of the impact

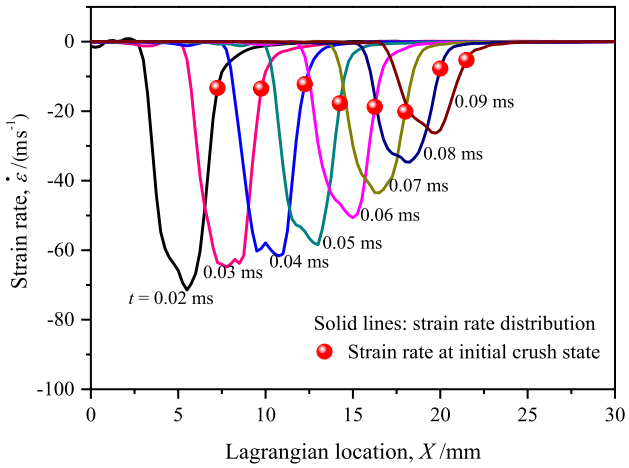

Fig. 12 Variation of local strain rate with Lagrangian location at different moments of the impact

is related to the strength of each layer of cells, which have inevitable randomness, anisotropy, and defects due to the cellular nature of foams, the corresponding local strain rate may vary with time during the impact process. Accordingly, the variation of the dynamic initial stress σ_0^{d} with the local strain rate is depicted in Fig. 13. This plot indicates that the dynamic initial crushing stress exhibits strain rate sensitivity. The dynamic initial crushing stress increases with increase of the strain rate with a nearly power-law trend, as also reported in Refs. [15, 19], expressed as

$$\sigma_0^{\mathrm{d}}(\dot{\varepsilon})/\sigma_0 = k(\dot{\varepsilon}/r)^n, \tag{7}$$

where the fitting parameters are determined in the present study to be $k = 0.942$, $r = 0.738\ \mathrm{ms}^{-1}$, $n = 0.136$, and $\sigma_0 = 5.90$ MPa, which is the plateau stress under quasistatic

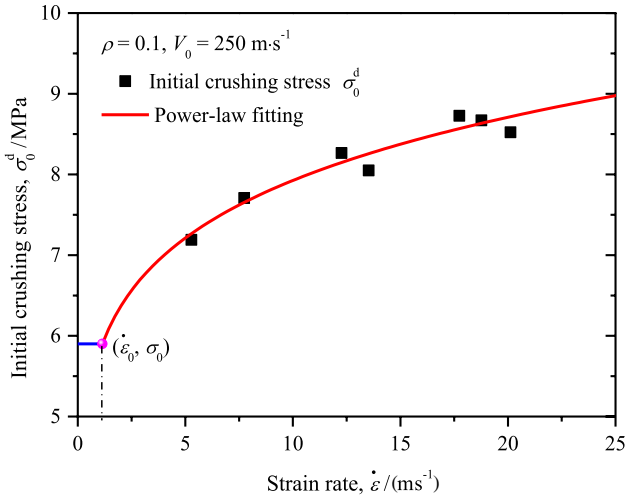

Fig. 13 Variation of initial crushing stress with strain rate

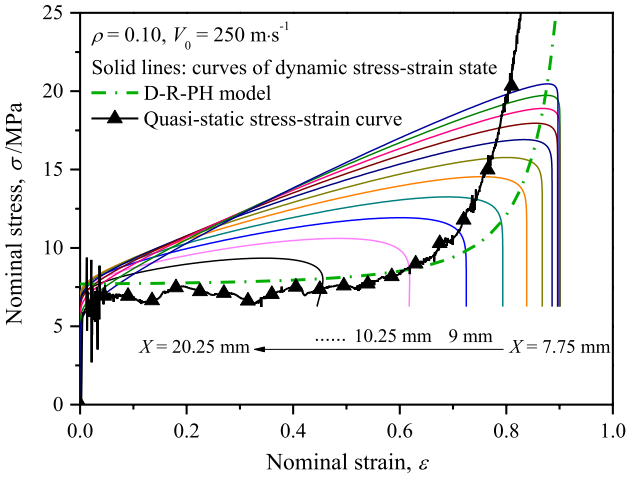

Fig. 14 Dynamic stress–strain history curves and quasistatic stress–strain curve of cellular material

compression, as illustrated in Fig. 13. With an increase of the local strain rate, the increasing trend of the initial crushing stress gradually slows down. In fact, when the impact velocity is high enough, further improvement of the loading velocity cannot obviously improve the strain rate of materials, or at least the magnitude remains almost unchanged. Thus, in the case of the dynamic behavior of cellular materials, the strain rate varies across a narrow range and the dynamic initial crushing stress changes only slightly. Therefore, the dynamic initial crushing stress is usually taken as a constant value for convenience [11, 21].

Note that the initial crushing stress σ_0^{d} drops to the value of the plateau stress σ_0 under quasistatic compression when the strain rate is below 1.14 ms^{-1}, since the strain rate ahead of the crushing front is constant and small enough to be neglected. Under a dynamic impact, the cells immediately ahead of the crushing front progressively collapse in a specific manner, since the inertia effect within the cell walls leaves no time for these cells to dissipate kinetic energy in a relatively weak region. Herein, the cells immediately ahead of the crushing front behave relatively rigidly compared with the quasistatic case. The region through which the crushing front has already passed is considered to be a compacted continuum with uniform stress distribution, and the inertial term $\rho_{\mathrm{f}} v^2/\varepsilon_{\mathrm{B}}$ dominates the shock stress σ_{B} in this region once the crushing front has passed.

4.3 Dynamic stress–strain states

Together with the time-history distributions of the local stress and local strain, the dynamic local stress–strain history curves of a cellular specimen can also be obtained, as shown in Fig. 14. As the crushing event advances, sectional cells experience a process successively: a rapid increase of stress to the dynamic initial crushing stress in the elastic stage, then plastic collapse of cells within the plastic deformation stage, and finally the unloading stage. The elastic properties of the cellular specimen dominate its mechanical behavior in the elastic and unloading stages, resulting in the consistent slopes of the curves in these two stages. A nearly linear chord, which is known as the Rayleigh chord when used to characterize the initiation of a plastic shock wave in stress wave theory [32], links the two turning points on the dynamic local stress–strain curves. Hence, the plastic deformation stage is controlled by the structural shock wave, which is strongly related to the impact velocity. The inflection point between the plastic deformation stage and the unloading stage is considered to be the dynamic stress–strain state point of the cellular specimen.

The obvious difference between the dynamic stress–strain states and the quasistatic stress–strain relation of the cellular specimen is depicted in Fig. 14, a phenomenon also confirmed in two-dimensional (2D) irregular honeycombs [13, 15]. The deformation mode of cellular materials exhibits strong dependence on the loading rate, and the formation mechanism and interaction of crushing bands dominate the response macroscopically [11]. Cellular materials are typical materials with inhomogeneous mesoscopic structure and high porosity. For such materials, an increase of the loading rate essentially enhances the micro-inertial effects, which play a significant part in enhancing the plastic strength of foams under high-velocity impact [37]. As the kinetic energy is dissipated, the transitional mode in which the deformation is a mixture of random shear bands in quasistatic compression and layerwise crushing bands under the dynamic impact of the cellular specimen occurs as the magnitude of the loading velocity gradually drops to moderate loading rates. It is observed that the dynamic stress–strain states predicted

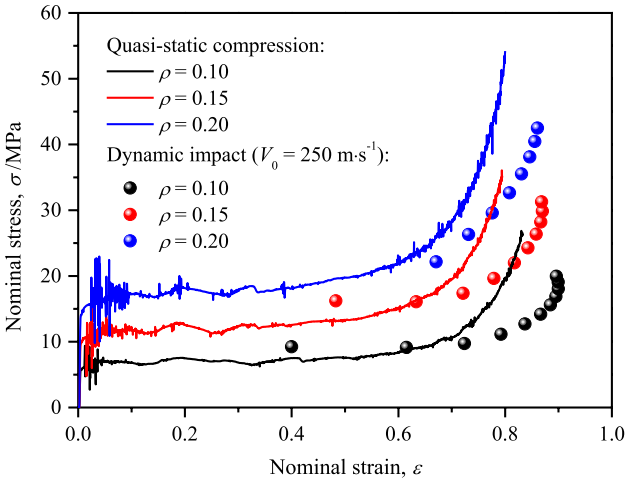

Fig. 15 Comparison of dynamic stress–strain states and quasistatic stress–strain curves of cellular materials with three different relative densities

by the D-R-PH shock model are in reasonable agreement with the results determined by the velocity-based analytical model in this study under high-velocity impact. It is also found that, when the impact velocity is attenuated to a certain range, the difference between the results obtained by the two methods gradually expands. This can be explained by the fact that shock models based on an idealized shock formation cannot characterize the mechanical behavior of cellular materials under moderate loading rates, since the transitional mode arises in the deformation pattern. Similarly, the method discussed herein provides an accessible and convenient route to investigate the behavior of cellular materials under dynamic loading. Further effort is required to reveal the mechanisms of deformation and stress wave propagation under moderate-velocity impact, since this issue remains unclear.

4.4 Effect of relative density on dynamic hardening behavior

One advantage of using a Voronoi structure instead of an experimental foam specimen is the controllability of the mesostructure, thus the relevant parameters of cellular materials can be investigated individually [38]. As an essential material parameter, the influence of the relative density on the dynamic behavior of the cellular specimen is considered in this section. By changing the cell-wall thickness of the Voronoi structure with given configuration, cellular specimens with three different relative densities are obtained. Using the velocity distribution-based analytical model, the dynamic stress–strain states of the cellular specimens with three relative densities are shown in Fig. 15. This figure indicates that the increasing trend of the shock stress becomes much steeper as the relative density is increased within the range of the densification strain, meaning that the dynamic hardening property of the cellular specimen is enhanced. On the mesoscopic scale, the mechanical performance (e.g., the plastic strength, strain-hardening behavior, and interaction of collapse cells) is highlighted, since high relative density of the cellular specimen corresponds to greater thickness of the cell-wall structures. Physically, strength reinforcement of the cell walls can be achieved by using base materials with strain-hardening and strain-rate-hardening properties [21]. Besides, it is worth mentioning that the speed of crushing front propagation does not obviously advance with the decrease in the compressible volume for the cellular specimen with higher relative density, which can be attributed to the competitive mechanisms of impact velocity attenuation and dynamic hardening behavior [21]. Hence, the crushing process is greatly sped up due to the enhanced energy absorption capacity of the cellular specimen with higher relative density. It is expected that further understanding of such dynamic behavior could contribute to crashworthiness design of cellular materials.

5 Conclusions

The dynamic crushing behavior of cellular materials is investigated numerically by using cell-based finite element models. The one-dimensional velocity distribution is extracted to reveal the evolution of the inhomogeneous deformation, capturing well the propagation of the crushing front through the cellular specimen under the initial velocity impact. An expression for the continuous velocity distribution is derived by adopting a Gaussian distribution to characterize the velocity gradient distribution features. Furthermore, a particle velocity-based analytical model is established to investigate the dynamic behavior of cellular materials effectively, in combination with equations for the conservation of mass and momentum in stress wave theory.

The densification strain behind the crushing front increases asymptotically to the maximum strain in solid states as the impact velocity is increased, showing good agreement with the results predicted by the D-R-PH shock model when the impact velocity is over 130 m/s. However, as the impact velocity drops, a difference appears between the densification strains obtained by the shock model and the velocity distribution-based analytical model, indicating a limitation of the shock model to describe behaviors of cellular materials under moderate loading rates. The investigation of the strain rate and dynamic initial crushing stress relations indicates that the dynamic initial crushing stress depends on the strain rate in a power-law manner under high-impact-velocity loading. After the propagation of the crushing front, the densification region of the cellular specimen is

basically a continuum with a uniform stress distribution and also exhibits sensitivity to the loading rate, since the inertia effect dominates the behavior in this compacted region.

The local stress–strain history distribution reveals the evolution of sectional deformation during crushing. Cells within cellular foams experience a rapid process from the precursor elastic behavior to the dynamic initial crushing stress as the crushing front arrives, then enter the shock stress state. The stress behind the crushing front corresponds to the loading rate along the linear Rayleigh chord whose slope characterizes the propagation speed of the crushing front. Compared with the quasistatic stress–strain curve of a cellular material, a significant difference is observed in the dynamic stress–strain curve, which can be explained based on the difference in deformation mechanisms and interactions of crushing bands. Furthermore, the dynamic hardening behavior is enhanced and the crushing process event advances more rapidly as the relative density of the cellular specimen is increased. The method established on the basis of particle velocity information herein to inversely determine the dynamic response of a cellular specimen may help to develop dynamic experimental techniques for such meso-inhomogeneous materials.

Acknowledgements This work was supported by the National Natural Science Foundation of China (Grants 11802002, 11772330, and 11372308), the Fundamental Research Funds for the Central Universities (Grant WK2480000003), and the Youth Foundation of Anhui University of Technology (Grant RD17100204).

Appendix A: Accuracy of Gaussian fitting for the velocity gradient

The width of the average of the velocity profile at a certain Lagrangian position, R_v, is introduced to evaluate the error of the velocity distribution fitting. It is found that the determined local strain distributions are basically coincident and the maximum relative error δ between the strains determined by the strain field method and the particle velocity-based method at one location, $X = 15$ mm for instance, is just 0.51% when the accuracy of the velocity fitting varies within 10%, i.e. the thickness of the crushing front ranges from 0.9 to 1.1 times the average cell diameter, as shown in Fig. 16. Actually, the relative error between the strain obtained using the velocity-particle model and the local strain field method still has an acceptable value (5.39%) even when the crushing front is enlarged to a thickness of two average cell diameters, as shown in Fig. 17. Therefore, the strain and stress results determined by the velocity model are relatively insensitive to the accuracy of the velocity gradient fitting.

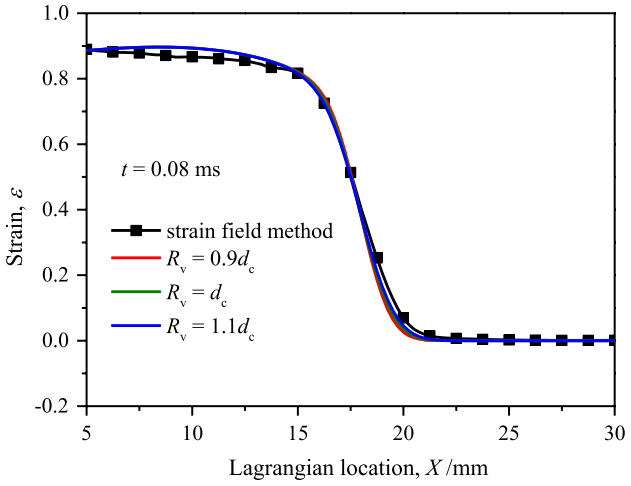

Fig. 16 Comparison of strain distribution obtained using different crushing front widths

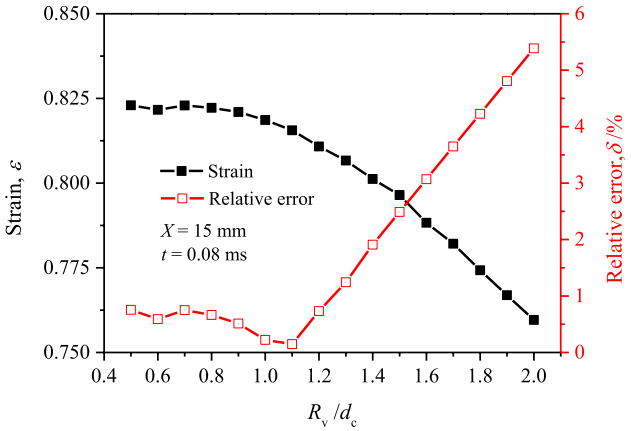

Fig. 17 Variation of the calculated strain and the relative error when fitting with different crushing front widths

Appendix B: Particle velocities at the free end

Initially, all the particles of the specimen move with an identical velocity V_0 towards the fixed plate. Once the impact event starts, a localized band of cell collapse forms from the impact end, then spreads to the distal end. Before the arrival of the elastic wave generated at the crushed end, the velocity of the particles at the free end of specimen remains at the original initial impact velocity. Then, the velocity starts to drop, since the kinetic energy of the specimen is gradually dissipated via plastic collapse of cells. The variation of the velocities obtained directly from the virtual experimental results and based on the velocity-based model proposed herein is depicted in Fig. 18.

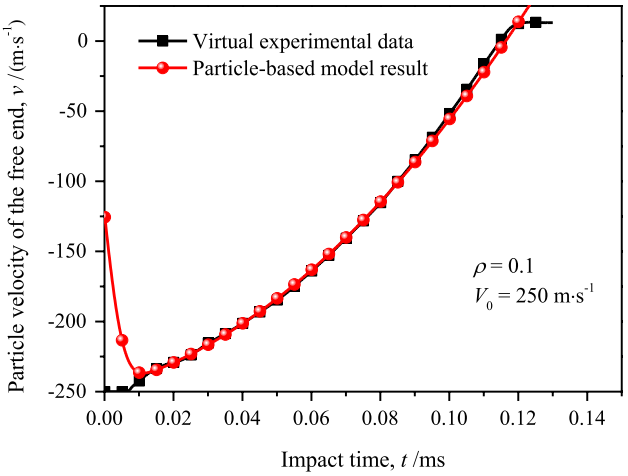

Fig. 18 Variation of particle velocities at free end with impact time

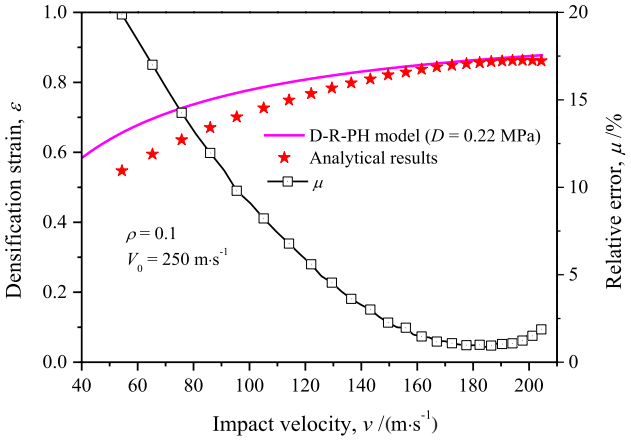

Fig. 19 Variation of densification strain with impact velocity and corresponding relative error

Considerable deviation is found for the initial condition calculated by Eq. (4). When the impact starts, the gap between the two velocities gradually shrinks, and the two basically coincide at the moment when the elastic wave propagates to the free end; i.e., the particle velocity-based model neglects the effect of the elastic loading and unloading waves that occur within the short initial stage.

Appendix C: The critical velocity of the D-R-PH model

The critical velocity of cellular materials can be physically defined as the deformation transition from the moderate-velocity mode to the shock mode. Actually, it is hard to give an accurate definition of the critical velocity, since this transition is not sharp. Essentially, the velocity at which the densification strain starts to depart from the predictions of the D-R-PH shock model differs from the definition of the critical velocity. The D-R-PH model can well characterize the dynamic behavior of cellular materials under high-velocity impact but may lose validity when the impact velocity is below the shock-induced value. Meanwhile, the particle velocity-based method proposed herein turns out to be reliable to characterize the behavior of cellular materials under a wide range of impact velocity. It is necessary to define a critical impact velocity to indicate the applicability of the D-R-PH model. Actually, when the impact velocity drops to around 100 m/s, the relative error μ between the densification strain predicted by the D-R-PH model and that determined by the particle velocity-based method is about 9.2 %, as illustrated in Fig. 19. Basically, impact velocities above 100 m/s can be treated appropriately as the shock-induced critical velocity.

References

1. Hanssen, A.G., Enstock, L., Langseth, M.: Close-range blast loading of aluminium foam panels. Int. J. Impact Eng. **27**, 593–618 (2002)
2. Ashby, M.F., Evans, A.G., Fleck, N.A., et al.: Metal Foams: A Design Guide. Butterworth, Heinemann (2000)
3. Degischer, H.P., Kriszt, B.: Handbook of Cellular Metals: Production, Processing, Applications. Wiley, Weinheim (2002)
4. Tatacipta, D., Annisa, J., Oktavia, K.E., et al.: Crashworthiness analysis of foam–filled square column considering strain rate effect of the foam. Thin Walled Struct. **129**, 365–380 (2018)
5. Tan, P.J., Reid, S.R., Harrigan, J.J., et al.: Dynamic compressive strength properties of aluminium foams. Part I—experimental data and observations. J. Mech. Phys. Solids **53**, 2174–2205 (2005)
6. Reid, S.R., Peng, C.: Dynamic uniaxial crushing of wood. Int. J. Impact Eng. **19**, 531–570 (1997)
7. Wang, L.L., Yang, L.M., Ding, Y.Y.: On the energy conservation and critical velocities for the propagation of a "steady-shock" wave in a bar made of cellular material. Acta Mech. Sin. **29**, 420–428 (2013)
8. Harrigan, J.J., Reid, S.R., Tan, P.J., et al.: High rate crushing of wood along the grain. Int. J. Mech. Sci. **47**, 521–544 (2005)
9. Pattofatto, S., Elnasri, I., Zhao, H., et al.: Shock enhancement of cellular structures under impact loading: part II analysis. J. Mech. Phys. Solids **55**, 2672–2686 (2007)
10. Lopatnikov, S.L., Gama, B.A., Haque, M.J., et al.: Dynamics of metal foam deformation during Taylor cylinder–Hopkinson bar impact experiment. Compos. Struct. **61**, 61–71 (2003)
11. Zheng, Z.J., Wang, C.F., Yu, J.L., et al.: Dynamic stress–strain states for metal foams using a 3D cellular model. J. Mech. Phys. Solids **72**, 93–114 (2014)
12. Liao, S.F., Zheng, Z.J., Yu, J.L.: On the local nature of the strain field calculation method for measuring heterogeneous deformation of cellular materials. Int. J. Solids Struct. **51**, 478–490 (2014)
13. Liao, S.F., Zheng, Z.J., Yu, J.L.: Dynamic crushing of 2D cellular structures: local strain field and shock wave velocity. Int. J. Impact Eng. **57**, 7–16 (2013)
14. Barnes, A.T., Ravi-Chandar, K., Kyriakides, S., et al.: Dynamic crushing of aluminum foams: part I—experiments. Int. J. Solids Struct. **51**, 1631–1645 (2014)

15. Wang, P., Zheng, Z.J., Liao, S.F., et al.: Strain-rate effect on initial crush stress of irregular honeycomb under dynamic loading and its deformation mechanism. Acta Mech. Sin. **34**, 117–129 (2018)
16. Sun, Y.L., Li, Q.M., McDonald, S.A., et al.: Determination of the constitutive relation and critical condition for the shock compression of cellular solids. Mech. Mater. **99**, 26–36 (2016)
17. Gaitanaros, S., Kyriakides, S.: On the effect of relative density on the crushing and energy absorption of open-cell foams under impact. Int. J. Impact Eng. **82**, 3–13 (2015)
18. Zou, Z., Reid, S.R., Tan, P.J., et al.: Dynamic crushing of honeycombs and features of shock fronts. Int. J. Impact Eng. **36**, 165–176 (2009)
19. Ding, Y.Y., Wang, S.L., Zheng, Z.J., et al.: Dynamic crushing of cellular materials: a unique dynamic stress–strain state curve. Mech. Mater. **100**, 219–231 (2016)
20. Sun, Y.L., Li, Q.M.: Dynamic compressive behaviour of cellular materials: a review of phenomenon, mechanism and modelling. Int. J. Impact Eng. **112**, 74–115 (2017)
21. Wang, S.L., Ding, Y.Y., Wang, C.F., et al.: Dynamic material parameters of closed-cell foams under high-velocity impact. Int. J. Impact Eng. **99**, 111–121 (2017)
22. Davison, L.: Fundamentals of Shock Wave Propagation in Solids. Springer, Berlin (2008)
23. Radford, D.D., Deshpande, V.S., Fleck, N.A.: The use of metal foam projectiles to simulate shock loading on a structure. Int. J. Impact Eng. **31**, 1152–1171 (2005)
24. Okabe, A., Boots, B., Sugihara, K., et al.: Spatial Tessellations: Concepts and Applications of Voronoi Diagrams. Wiley, London (2000)
25. Barber, C.B., Dobkin, D.P., Huhdanpaa, H.: The quickhull algorithm for convex hulls. ACM Trans. Math. Softw. **22**, 469–483 (1996)
26. Song, Y.Z., Wang, Z.H., Zhao, L.M., et al.: Dynamic crushing behavior of 3D closed-cell foams based on Voronoi random model. Mater. Des. **31**, 4281–4289 (2010)
27. Zhang, X.Y., Tang, L.Q., Liu, Z.J., et al.: Yield properties of closed-cell aluminum foam under triaxial loadings by a 3D Voronoi model. Mech. Mater. **104**, 73–84 (2017)
28. Li, L., Xue, P., Chen, Y., et al.: Insight into cell size effects on quasi-static and dynamic compressive properties of 3D foams. Mater. Sci. Eng. A Struct. **636**, 60–69 (2015)
29. Shi, X.P., Liu, S.Y., Nie, H.L., et al.: Study of cell irregularity effects on the compression of closed-cell foams. Int. J. Mech. Sci. **135**, 215–225 (2018)
30. ABAQUS, Version 6.11. Abaqus Analysis User's Manuals, Simulia, Dassault Systmes, Rising Sun Mills, USA
31. Harrigan, J.J., Reid, S.R., Yaghoubi, A.S.: The correct analysis of shocks in a cellular material. Int. J. Impact Eng. **37**, 918–927 (2010)
32. Wang, L.L.: Foundations of Stress Waves, 2nd edn. National Defense Industry Press, Beijing (2005)
33. Li, L., Zhao, Z.Y., Zhang, R., et al.: Dual-level stress plateaus in honeycombs subjected to impact loading: perspectives from bucklewaves, buckling and cell-wall progressive folding. Acta Mech. Sin. (2018). https://doi.org/10.1007/s10409-018-0800-1
34. Deshpande, V.S., Fleck, N.A.: High strain rate compressive behaviour of aluminium alloy foams. Int. J. Impact Eng. **24**, 277–298 (2000)
35. Mukai, T., Miyoshi, T., Nakano, S., et al.: Compressive response of a closed-cell aluminum foam at high strain rate. Scr. Mater. **54**, 533–537 (2006)
36. Wang, L.L., Ding, Y.Y., Yang, L.M.: Experimental investigation on dynamic constitutive behavior of aluminum foams by new inverse methods from wave propagation measurements. Int. J. Impact Eng. **62**, 48–59 (2013)
37. Fang, Q., Zhang, J.H., Zhang, Y.D., et al.: A 3D mesoscopic model for the closed-cell metallic foams subjected to static and dynamic loadings. Int. J. Impact Eng. **82**, 103–112 (2015)
38. Wu, H.X., Liu, Y., Zhang, X.C.: In-plane crushing behavior and energy absorption design of composite honeycombs. Acta Mech. Sin. **34**, 1108–1123 (2018)